Volume 1 | Number 1 | Jan 2013 | Pages 1–100

## RSC Advances

www.rsc.org/advances

# Journal Name

## ARTICLE

# Tailoring base catalyzed synthesis of palm oil based alkyd resin through CuO nanoparticles

Huei Ruey Ong[a,b], Md. Maksudur Rahman Khan[a*], Ridzuan Ramli[b], Md. Wasikur Rahman[a] and Rosli Mohd Yunus[a]

Palm oil based alkyd resin was synthesized by alcoholysis–polyesterification process over base catalyst tailored by copper oxide (CuO) nanoparticles. In the present paper we synthesized CuO sol in glycerol and subsequently used in alkyd resin synthesis. The formation of the alkyd resin was confirmed by FTIR, Raman, $^1$H–NMR and $^{13}$C–NMR methods and its molecular weight was determined by Gel permeation chromatograph (GPC).The antimicrobial activity of the pseudo–homogeneous additive was determined via Kirby–Bauer Method and The CuO stability was determined by X–ray absorption near edge structure spectroscopy (XANES). The addition of CuO nano–sol to the conventional homogeneous base catalyzed system explored a new catalytic route for the preparation of bioresin from vegetable oil reducing the reaction time, as well as adding the antimicrobial properties to the resin.

## Introduction

Rapid scarcity of fossil fuels as well as a threat to the environment associated with the application of petroleum–based monomers for the synthesis of alkyd resin can be resolved by the use of renewable resources and availability of raw materials like vegetable oils of plant origin. Alkyd resin is mainly used in the formulation of paints, varnishes, lacquers, adhesives and composites[1-3]. The main reactions for the synthesis of alkyd resins involve the alcoholysis of the oil by a part of the polyol used followed by esterification with a polyacid and the remainder of the polyol. The most common polyol and diacid component are glycerol and phthalic anhydride, respectively[4]. Homogeneous base catalysts, such as Ca(OH)$_2$, KOH, NaOH, LiOH or heterogeneous base catalysts, such as CaO, ZnO/Alumina, calcium carbonate are reported to conduct the reaction at ~240°C. After the first step of the reaction, the products contain 40–60% monoglyceride (MG)[5, 6] which is important to homogenise the reaction medium and allow the reaction to be proceeded to polyesterification[7] and the rest are diglyceride (DG) and triglyceride (TG). Monoglycerides, the glycerol monoesters of fatty acids, are important modifying agents in the manufacture of alkyd resins, polymers and lubricants; need to raise their yields. The time required in heterogeneous system in acquiring

maximum MG yield is longer compared to homogeneous one. Lowering the activation energy as well as shortening the reaction time in alcoholysis is crucial to make the process effective. Ferretti, et al.[5] showed that MgO is a potential heterogeneous catalyst in MG preparation due to its high surface area. The process yields ~77% of MG after 2 h of reaction; higher than the liquid–base–catalyzed homogeneous process (40–60%). The utility of the catalyst in alcoholysis reaction no further explored for polyesterification reaction. Nano–structured heterogeneous catalyst is promising now–a–days due to its ultrafine size and high surface area. The inclusion of nano–structured heterogeneous catalyst in homogeneous catalysis system can provide a new catalytic environment for alkyd resin synthesis. Moreover, the catalyst remaining in the polymer matrix after polyesterification, additionally acts as a property enhancer, such as antimicrobial would be much interesting; not yet reported. A number of metal oxide nanoparticles such as zinc oxide (ZnO)[8], titanium dioxide (TiO$_2$)[9], copper oxide (CuO)[10] etc. as antimicrobial agents have drawn attention in the recent years because they show strong activity against bacteria even at low concentration[11] and regarded as non–toxic materials[12]. CuO nanoparticles, of them, attracted more attention due to its high catalytic activity and low cost[13, 14]. The incorporation of nanoparticle into the polymer matrix usually performed through mixing after formation of polymer[8, 10, 15]. Delgado, et al.[10] embedded copper (Cu) and CuO nanoparticles in polypropylene as antimicrobial agents and found that, CuO are more effective than Cu. Besides, the antimicrobial activity of ZnO nanoparticle in polypyrrole/chitosan blend was studied by Ebrahimiasl, et al.[8] and reported that it is effective against bacteria especially for *Pseudomonas aeruginosa*. Our attempt is to promote catalytic activities of liquid bases with Cu

a. Faculty of Chemical & Natural Resources Engineering, Universiti Malaysia Pahang, 26300 Gambang, Pahang, Malaysia. E–mail: mrkhancep@yahoo.com
b. Malaysian Palm Oil Board (MPOB),No. 6, Persiaran Institusi, Bandar baru bangi, 43000 Kajang, Selangor, Malaysia.
† Footnotes relating to the title and/or authors should appear here.
Electronic Supplementary Information (ESI) available: [details of any supplementary information available should be included here]. See DOI: 10.1039/x0xx00000x

nanoparticles on chemical conversion of palm oil into alkyd resin. Palm is the most important agriculture crop in Malaysia, since Malaysia is one of the main palm oil producers and exporting countries in the world[16, 17].

In this context, a new catalytic environment comprising with NaOH and CuO nanoparticles was explored in alkyd resin synthesis. The CuO nanoparticle was prepared in glycerol medium and the antimicrobial activity of CuO incorporated alkyd resin was examined.

## Results and Discussion

### Preparation of alkyd resin

The end point of alcoholysis was determined via methanol solubility test. The reaction mixtures were withdrawn at different time intervals to determine the solubility of the samples. Time required at the end point of each catalyzed reaction was presented in Figure 1. It can be seen that, CuO–NaOH catalyzed reaction (A100, A200 and A300) significantly reduced the reaction time. A200 catalyzed system showed shortest reaction time, while further addition of CuO, did not influence the system significantly. Besides that, determination of end point is useful in preventing prolonged alcoholysis reaction time and it can lead to aggravation of side reaction such as formation of polyglycerols[18].

In alcoholysis reaction, the reaction occurred as fatty acid ligands of TG combined with the glycerol to produce MG and DG. The role of $OH^-$ anion from NaOH was to extract hydrogen from glycerol for the formation of glyceroxide. The $Na^+$ cation is to participate in the stabilization of negatively charged intermediates (glyceroxide). Besides that, it also used to activate the TG molecule (polarization of C=O bond of TG) and facilitate the attack of glyceroxide anion to the positively charge carbonyl carbon in TG [19]. For the CuO–NaOH catalyzed reaction, CuO nanoparticle can act as catalyst providing the basic sites on its surface. Ferretti, et al. [19] reported the catalytic activity of MgO in the alcoholysis of fatty acid methyl ester (FAME), where the synthesis of monoglycerides was promoted mainly on strongly basic low coordination $O^{2-}$ surface sites. Moreover, for CuO-NaOH system, CuO may assist $Na^+$ cations with surface positive charges as well as create possibly higher electronegativity deviation resulting in higher catalytic activity. Further study will be required to elucidate the mechanism of the reaction in the CuO-NaOH catalysed system.

The second step is polyesterification which is a condensation polymerization reaction. The progress of polyesterification was monitored by periodic determination of the AV via the titration of unreacted carboxylic acid groups. The AV of different catalyzed reactions at different time intervals was shown in Figure 2. The plot indicates that as the reaction progressed, the AVs decreased. The decrease in acid values was more rapid during the early stages of the reaction than that during the later stages of the reaction. Similar trends were also reported elsewhere[20-23]. These changes in acid values during polyesterification reaction have been explained on the

basis of different reactivity of primary and secondary hydroxyl groups of MG[24]. Since primary hydroxyl groups react faster than secondary groups, it is believed that the rapid decrease in acid values at the early stages due to primary hydroxyl groups, while that at the later stages for secondary groups[20]. In addition, three–dimensional network of alkyd resin is probably formed at the later stages of polyesterification due to cross–linking of alkyd chains as the viscosity of the reaction medium is increased[25].

The influence of CuO addition is clearly evident at the early stage of the reaction as revealed from Figure 2. The initial rates for each catalyzed system were determined by following three–point method[26] and the data are presented in Figure 2 (Table, inset). It can be observed from the figure that the initial reaction rates of CuO catalyzed reactions (A100, A200 and A300) are significantly higher compared to A0. The initial reaction rates of A100, A200 and A300 were found to be 10.40, 12.79 and 13.07 $mgKOHg^{-1}s^{-1}$ (Figure 2, Table inset). However, it is noticed that the initial reaction rates of A200 and A300 were almost similar. Apart from that, it can be seen that A200 catalyzed reaction reached equilibrium earlier (60 min) than others (Figure 2). In addition, the DP of the reaction was calculated from the AV by using Equations 1 and 2. The effect of CuO content on DP was presented in Figure 2. It can be seen that, the DP value increased as the reaction progressed. The curve exhibits two distinct portions, where the initial linear portion corresponds to bond formation between primary hydroxyl groups of MG and PA. It is evident from Figure 2 that the rates of this step for CuO-NaOH catalyzed systems were significantly higher than that of the conventional NaOH catalyzed reaction. The increase of CuO concentration demonstrated the increase in DP. The second curved portion corresponds to bond formation between secondary groups of MG and PA where the DP value of A200 was higher compared to others up to 120 min of reaction time. In this context, A200 was selected as optimum catalytic system.
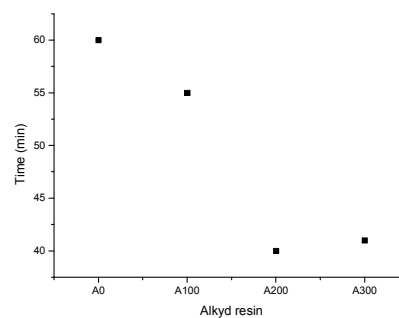


Figure 1. Effect of different catalytic systems on alcoholysis (reaction time).
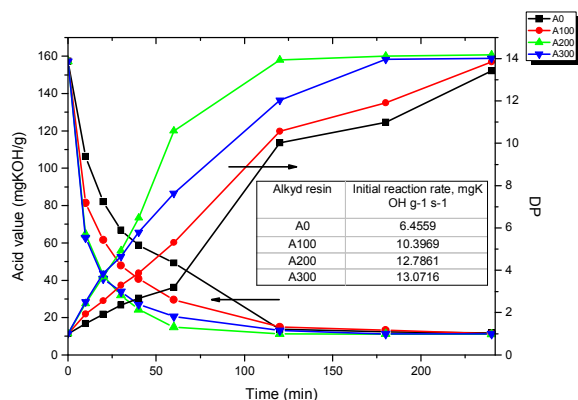
Figure 2. Plot of acid value and DP against reaction time for different catalysis systems during polyesterification process (■A0, ●A100, ▲A200 and ▼A300). Table of initial reaction rates is shown inside the figure.
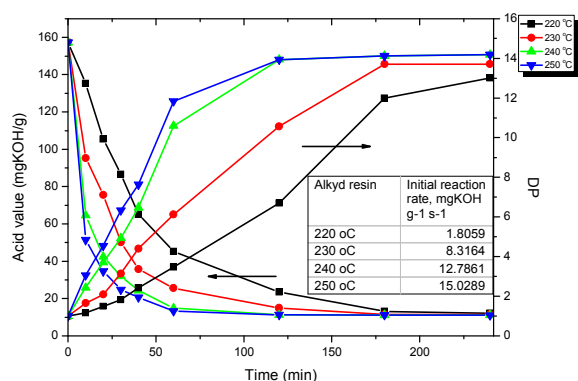


Figure 3. Plot of acid value and DP against reaction time for different temperature during A200 catalysed polyesterification process (■220 °C, ●230 °C, ▲240 °C and ▼250 °C). Table of initial reaction rates is shown inside the figure.

The effect of temperature during A200 catalysed polyesterification was presented in Figure 3. It can be seen that, temperature influenced the reaction significantly, especially during early stage of the reaction. The initial rate of the reaction for 220, 230, 240 and 250 °C was 1.8059, 8.3164, 12.7861 and 15.0289 mgKOHg$^{-1}$s$^{-1}$, respectively (Figure 3, Table inset). However, in comparison to A0 (at 240 °C) catalyzed reaction, the initial rate of reaction catalyzed by A200 at 230 °C was almost similar and reached equilibrium at 120 min. Besides that, DP value of sample at 230 °C for A200 was higher than A0 at 240 °C. The result suggested that the CuO-NaOH catalyst system required lower temperature to achieve similar DP compared to conventional NaOH catalyzed system. Furthermore, it was found the initial rate of the reaction was increased with the increase in temperature upto 240 °C for A200 and in further increase in temperature the AV and corresponding DP values were almost unchanged. In this

context, 240 °C was chosen as the optimum condition considering rapid early stage reaction and to shorten the reaction period.

## Characterization of alkyd resin

### FTIR analysis

The FTIR spectra of oil, alkyd and copper incorporated alkyd resin are shown in Figure 4. The spectrum of oil was different compared to alkyd resin. In the FTIR spectrum of palm oil (Figure 4, curve i), a broad band was observed at 3540–3200 cm$^{-1}$ corresponding to O–H stretching vibration[23]. The spectrum also showed a strong absorption in the region of 3030–2840 cm$^{-1}$ due to C–H stretching[27, 28]. The absorption bands at 1740–1725 cm$^{-1}$ was attributed to C=O and that at 1240–1100 cm$^{-1}$ for C–O–C stretching vibration of ester group in triglyceride molecule[29]. Absorption at 1465–1445 cm$^{-1}$ was assigned to C–H bending. In addition, absorption peak at 722 cm$^{-1}$ was due to the presence of unsaturation in fatty acid[30].

The FTIR spectra of alkyd resin (Figure 4, curve ii and iii) indicated the presence of ester linkages and other characteristic peaks. It is important to note that a new characteristic peak of ester group at 1280–1260 cm$^{-1}$ (C–O–C stretching)[22] was appeared that was absent in the spectrum of oil. Besides that, palm oil showed a peak at 1748 cm$^{-1}$ for C=O stretching, whereas, in the case of synthesized resin that appeared at 1735 cm$^{-1}$. Apart from that, characteristic peak at 743 cm$^{-1}$ corresponds to C–H bending of aromatic ring contributed by phthalate units[28]; confirmed the formation of alkyd resin via polyesterification process[23, 27]. Furthermore, the stretching frequencies of the spectra of A0 (Figure 4, curve ii) and A200 (Figure 4, curve iii) were almost the same. However, slight shifts of ester group (C–O–C stretching) and C–H bending of aromatic ring were noticed, from 1270 and 743 cm$^{-1}$ for A0 to 1266 and 735 cm$^{-1}$ for A200, respectively, suggesting the interaction (electrostatic interaction/hydrogen bonding) between polymer matrix and inorganic material (CuO)[31].
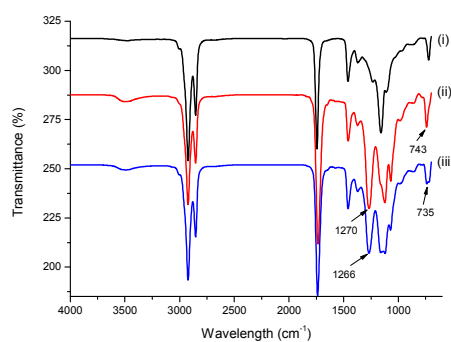


Figure 4. Infrared spectra of (i) oil, (ii) A0 and (iii) A200.

### Raman analysis

Raman spectroscopy is one of the non–destructive analyses used to study the bonding interaction, crystallinity, defects, and dislocations of nanomaterials such as graphene, metal oxide, several polymer etc[32, 33]. In order to study the

interaction occurred between the CuO and alkyd resin, in addition to FTIR spectra; we also examined the Raman spectra of alkyd resin (A0) and CuO–alkyd (A200) (Figure 5). Apart from that, CuO standard–alkyd was prepared by mixing 1 wt% of CuO standard powder with alkyd resin (A0) for investigation. The spectrum of CuO standard–alkyd was also presented in Figure 5. The Raman spectra were recorded in the range 0–4000 $cm^{-1}$. From the Figure, it can be seen that, the Raman frequency of all samples were almost similar. The O–H stretching was observed in the region of 3750–3300 $cm^{-1}$[34]. The band at 3200–3050 $cm^{-1}$ was attributed to =(C–H)[35] and that at 3000–2800 $cm^{-1}$ for C–H stretching[34]. Band at 1820 $cm^{-1}$ was assigned to C=O stretching[34]. The peak at 1635 $cm^{-1}$ and 1400 $cm^{-1}$ were corresponded to C=C[36-38] and $CH_2$, $CH_3$[36, 38]. The band for C–O–C was at 1250–1150 $cm^{-1}$ [36]. The band at 1050–950 $cm^{-1}$ and 725–670 $cm^{-1}$ were attributed to $CH_2$, C–C[36] and deformation of C–H[34, 39]. As seen from the Figure, the peak of C–O–C at 1190 $cm^{-1}$ (A0) was shifted to 1175 $cm^{-1}$ (A200), which might be due to the influenced of CuO. Apart from that, it is noticed that the band intensity of alkyd resin functional groups were reduced in the Raman spectra of A200 and CuO standard–alkyd. This is due to the fluorescence nature of inorganic material (CuO) in the sample, which overwhelms the weaker scattering bands of alkyd. This is in consistent with literature findings for using other materials like molybdenum oxide, graphene oxide and graphene[36, 40, 41]. In addition, the appearance of CuO peaks through Raman spectrum was not confirmed, as in the narrow scan at 200–800 $cm^{-1}$. The CuO peaks (usually at 295, 340 and 630 $cm^{-1}$) were not detected, which might be due to the low concentration of CuO in our samples.
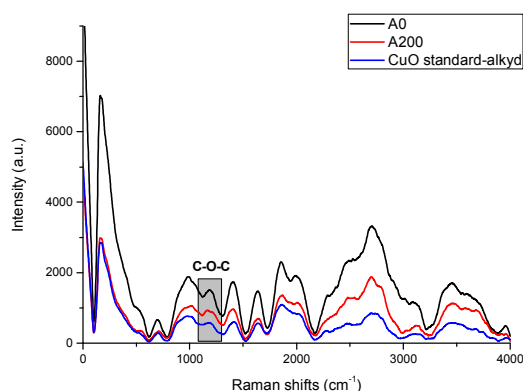


Figure 5. Raman spectra of A0, A200 and CuO standard–alkyd.

**NMR analysis**

Figure 6 shows the ^{1}H–NMR and ^{13}C–NMR spectra of palm oil–based alkyd resins and the formation of alkyd resin is confirmed by the appearance of new peaks in comparison with the spectra of palm oil, which presented in Figure S1. The methylene (–$CH_2$–) protons adjacent to hydroxyl groups in glycerol are seen at 3.50–3.80 ppm (Figure 6a). The downfield shifted of –$CH_2$– groups in the glyceride unit (4.12–4.32 ppm) was observed which probably due to reaction of hydroxyls

with PA causing the more electron withdrawing from the ester to be presented[29]. The peaks at 7.30–7.85 ppm are attributed to the resonance of –OOC–CH…CH–COO– protons from the PA moiety, confirming the incorporation of the PA. In ^{13}C–NMR spectra (Figure 6b), a pronounced difference between the carbonyl ester of the pendent of oleate/palmitate and the phthalate ester can be observed at 173.00–175.00 ppm and 168.35–169.80 ppm, respectively. It is also observed the appearance of smaller peaks at 61.00–74.00 ppm corresponds to the methylene groups (–$CH_2$–) of the glyceride[21, 29].

**Molecular weight characterization**

Table 1 presents the weight average molecular weight ($M_w$) and molecular weight distributions (MWD) of the alkyd resin at various stage of the polymerization reaction. It can be seen that, the $M_w$ of the samples A0 and A200 increased as reaction progressed. The low molecular weight of alkyds was observed at the beginning of the reaction, which attributed to the low rate of polymerization. Increase in polymerization rate resulted in increased molecular weight in the later stage. The observation is in agreement with literature reported for various vegetable seed oil alkyds, where molecular weight increased as reaction progressed[42, 43]. Similarly, the MWD values were increased as reaction progressed as well as DP increased. This evidenced the formation of linear polymer in early stage and three–dimensional network of alkyd resin in later stage. The MWD values of A0 and A200 at 180 min were 2.83 and 2.81, respectively. The size distribution of the samples was almost the same, while their $M_w$ were different. The $M_w$ of A0 and A200 at 180 min were 2723 and 2403 g/mol, respectively. A200 exhibits lower $M_w$ than A0, indicates that it is more suitable to use as chief ingredient in paint and surface coating, where low $M_w$ polymer shows better performance in coating[44, 45].

**Stability of CuO nanoparticle**

The XANES spectra can provide valuable information regarding oxidation states of copper and the composition of the samples at different oxidation states. The spectra of Cu–based nanoparticles were investigated in order to understand the stability of CuO nanoparticles before and after the reaction shown in Figure 7. As seen from the Figure, the XANES spectra of the two CuO nanoparticle samples revealed similar features to the CuO standard. Furthermore, the relative compositions of the samples were elucidated and the XANES spectra were deconvoluted with considering the contribution of Cu, CuO and $CuCl_2 \bullet 2H_2O$. A linear fitting of the composition of two samples (before and after reaction) was performed and the simulation results were summarized in Table 2. It can be seen that, the phase of CuO nanoparticles prepared by the mentioned method dominated in CuO phase after the reaction may be due to the oxidation of pure Cu (17 wt%) during the polymerization reaction. The composition of CuO before and after the reaction consists of ~83 and ~100 wt% CuO, respectively.

# Journal Name

## ARTICLE
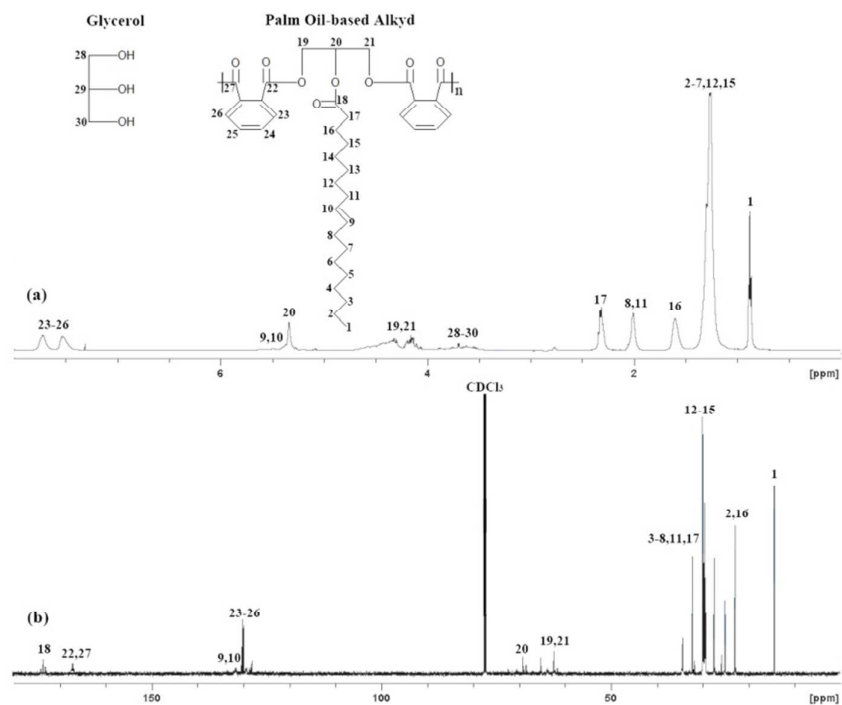


Figure 6. ^{1}H–NMR (a) and ^{13}C–NMR (b) of palm oil–based alkyd resin.
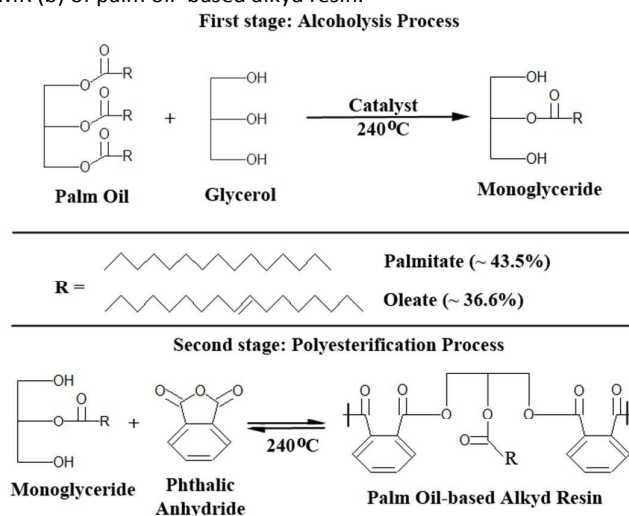


Scheme 1. Synthetic pathway of palm oil–based alkyd resin (alcoholysis–polyesterification process).

Table 1. Molecular weights and molecular weight distributions of palm oil alkyd resin with CuO (A200) and without CuO nanoparticles (A0) at various stage of the reaction.

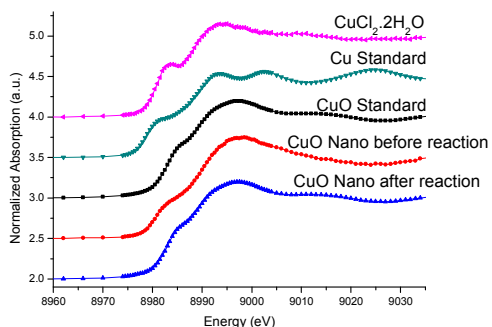| Time (min) | A0 | | A200 | |
|---|---|---|---|---|
| | $M_w$ (g/mol) | MWD | $M_w$ (g/mol) | MWD |
| 0 | 739 | 1.23 | 739 | 1.23 |
| 30 | 1418 | 1.74 | 1402 | 1.52 |
| 60 | 1739 | 1.85 | 1643 | 1.72 |
| 120 | 2191 | 2.24 | 2105 | 2.16 |
| 180 | 2723 | 2.83 | 2403 | 2.81 |



Figure 7. XANES spectra at the Cu K edge of Cu standard, CuO standard, $CuCl_2 \bullet 2H_2O$, CuO nanoparticle before reaction and CuO nanoparticle after reaction.
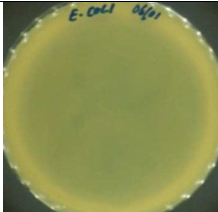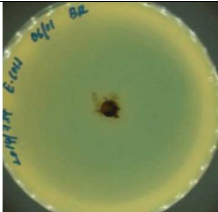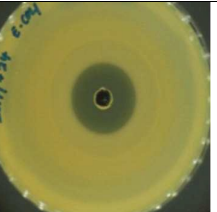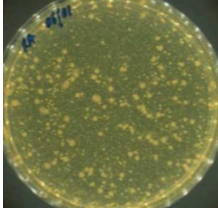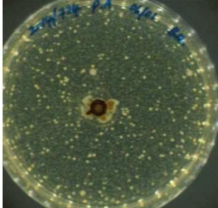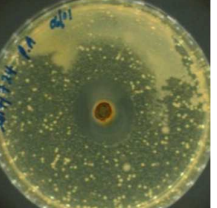
Table 2 Composition of Cu/O obtained from the linear fitting with the sample CuO nanoparticle before and after the reaction.

| Nanoparticle | CuO (wt%) | Cu (wt%) |
|---|---|---|
| Before reaction | 82.62±0.15 | 17.38±0.13 |
| After reaction | 100 | 0 |

### Antimicrobial study

The antimicrobial activity of A0 and A200 against microorganism was tested based on zone of inhibition as presented in Table 3. Gram Negative (*Escherichia coli, Pseudomonas aeruginosa, Salmonella sp.)* and Gram Positive (*Staphylococcus aureus*) microorganisms were selected for their activity test. The zones of inhibition of A200 were tested after 24 h of the incubation at 32.5 °C and found to be 23 mm for *Escherichia coli,* 25 mm for *Pseudomonas aeruginosa,* 15 mm for *Staphylococcus aureus* and 40 mm for *Salmonella sp.* , whereas, the control and A0 samples did not show any zone of inhibition (Table 3). A200 showed good antimicrobial activity. However, the mechanism of bactericidal is still not well known. It might be due to the strong bind of nanoparticle to cell membrane or electron donor groups such as sulphur and nitrogen in biological molecules, which resultant the disruption in the bacterial cell wall and causes the cells death[46-48]. Apart from that, the formation of copper–peptide complex may disturb the metabolism of bacterial cells and their power functions such as permeability and respiration which will also cause death of bacterial cells[48, 49]. Overall comparison of the microbial reduction rates in the present study revealed Gram negative bacteria to be more susceptible to the antimicrobial effects of Cu ions than Gram positives, presumably due to their thinner wall, which may allow more rapid absorption of the ions into the cell[50, 51].

Table 3 Antimicrobial activity of A0 and A200

| Challenge Microorganism | Diameter for zone of inhabitation | | | Zone of Inhibition (Diameter, mm) |
|---|---|---|---|---|
| | Control | Alkyd resin | CuO incorporated alkyd resin | |
| *Escherichia coli* | | | | 23 |
| *Pseudomonas aeruginosa* | | | | 25 |

*Staphylococcus aureus*

*Salmonella sp.*

15
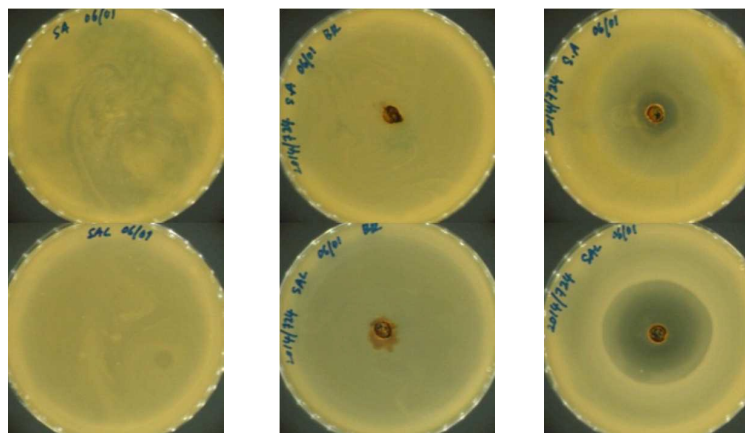
40

## Conclusions

Palm oil based alkyd resin was successfully synthesized by homogeneous base catalysed system incorporated with CuO nanoparticles. The addition of CuO nano–catalyst to the conventional NaOH catalytic system enhanced the catalytic behaviour of alcoholysis–polyesterification process reducing the reaction time for both alcoholysis and polyesterification reactions. The preparation of alkyd resin was confirmed by the formation of ester linkages evidenced by FTIR, ^{1}H–NMR and ^{13}C–NMR. The antimicrobial activity of A0 and A200 were determined via Kirby–Bauer Method and A200 posed better antimicrobial activity compared to A0. In addition, the molecular weight of alkyd demonstrated valuable information that the sample with lower $M_w$ (A200) is more suitable for surface coating application. The stability of CuO nanoparticle during the alkyd resin synthesis was examined and found that the state of CuO was unchanged throughout the whole experiment; results that CuO nanoparticle can be a potential co–catalyst as well as antimicrobial agent for alkyd resin synthesis.

## Experimental section

### Materials

Copper (II) chloride salt ($CuCl_2 \cdot 2H_2O$), hydrazine monohydrate (64%), ethanol (99.9%), anhydrous methanol, sodium hydroxide, glycerol, dimethyl sulfoxide (DMSO), copper (II) oxide (97%), copper (I) oxide (99.99%), *Escherichia coli* (ATCC 8739), *Pseudomonas aeruginosa* (ATCC 9027), *Staphylococcus aureus* (ATCC6538) and *Salmonella sp.* (ATCC 14028) were obtained from Sigma–Aldrich, Malaysia and used without further purification. Refined palm oil was provided by Malaysian Palm Oil Board (MPOB), Malaysia.

### Preparation of copper nanoparticles

The copper sol was synthesized by sol–gel method at room temperature reported elsewhere[14, 52, 53]. In brief, the required amount of $CuCl_2 \cdot 2H_2O$ was dissolved in 44 mL glycerol followed by 6 mL of hydrazine solution injected into the mixture drop–wise and the concentration of copper precursor

in the sol was maintained in the range of 100–300 mg/L. Prior to this, the hydrazine solution of 7.062 mM was prepared by diluting 64% hydrazine monohydrate in ethanol. The solution was stirred continuously for 10 h at room temperature. The formation and chemical state of copper nanoparticle was confirmed by using XANES.

### Preparation of alkyd resin

Alkyd resin was synthesized by alcoholysis of palm oil with glycerol followed by polyesterification. During alcoholysis, 100 g of palm oil was heated at 240 °C and 22.2 g of glycerol (molar ratio of glycerol/oil = 2:1) was incorporated into the system under constant stirring. Thereafter, 0.3 g of NaOH was added and the reaction was conducted under nitrogen purging. MG formation was determined via methanol solubility test[18]: Reaction mixture (1 mL) was withdrawn from reactor and cooled at room temperature prior to 2 mL of anhydrous methanol addition. Complete solubility of reaction mixture in methanol confirmed the 'end point' of alcoholysis and the reaction mixture was allowed to cool down at 140 °C. Thereafter, fine phthalic anhydride (PA) (38.7 g) was added into the reaction mixture to initiate the polyesterification process. The reaction temperature was maintained at 240 °C under nitrogen atmosphere. The samples were withdrawn at different time intervals to determine the acid value (AV) accordingly by ASTM D 1639–90 to monitor the progress of the reaction[23]. The reaction mixture was quenched to room temperature when the AV reached ~10. For the preparation of alkyd resin catalysed by CuO–NaOH system, pure glycerol was substituted by the as–prepared copper sol in glycerol in various concentrations, i.e., 0, 100, 200 and 300 mg/L were labelled as A0, A100, A200 and A300, respectively. The synthetic pathway of alkyd resin is presented in Scheme 1.

### Average degree of polymerization determination

The acid value of in–process samples withdrawn were determined by titrating method. The extent of the reaction, P and average degree of polymerization, DP were calculated on the basis of acid value using the following equation[54, 55]:

$$P = (C_0 - C_t)/C_0 - -(1)$$
$$DP = (1 - P)^{-1} - -(2)$$

Where $C_0$ is the initial acid value and $C_t$ is the acid value at time, t of the reaction.

### NMR spectroscopy

**13C NMR.** Spectra were recorded on high resolution spectrometers (AVANCE III; Bruker, Karlsruhe, Germany) located at the central laboratory (Universiti Malaysia Pahang, Malaysia) operating at a carbon–13 frequency of 500 MHz. Spectra were recorded at concentrations of 10–20% (w/v) (50–100 mg of sample in 0.5 mL of chloroform–*d*) using 5 mm NMR tubes at controlled temperatures of 30±0.1 °C in the broadband proton decoupling mode. Full 13C NMR spectra were obtained with the following acquisition parameters: 16 K data points, spectral width 200 ppm, acquisition time 0.37 s, relaxation delay 5 s, pulse width 45° and 256–3000 scans. High resolution carbonyl spectra were recorded with 16 K data points, spectral width 10 ppm, acquisition time 12–20 s, relaxation delay 5 s and pulse width 45–90°. Free induction decays (FIDs) were transformed by zero filling up to 32 K data points to yield a digital resolution of 0.05–0.08 Hz per point. All FIDs, prior to Fourier transformation (FT), were filtered using an exponential multiplication (0.2–0.4 Hz line broadening) for sensitivity enhancement. The peak intensities of the high resolution 13C NMR carbonyl spectra were accurately quantified using the Linesim (Bruker) curve resolute ion program.

**1H NMR.** Samples (20 μL) were placed in 5 mm NMR tubes and dissolved in chloroform–*d* (0.7 mL) and DMSO–*d6* (20 μL). The chemical shifts were referred indirectly to TMS signal (δ=0.0 ppm) by assigning the residual signal from mono protonated $CHD_2Cl_3$ to 7.26 ppm. One–dimensional spectra were recorded on Bruker AM400 instrument (Central Laboratory, Universiti Malaysia Pahang, Malaysia) operating at 400.13 MHz.

### FTIR spectroscopy

The structural information of the samples (oil, A0 and A200) were attained by FTIR Spectrometer (Spectrum 100 model, Perkin Elmer brand) equipped with an attenuated total reflectance (ATR) device in the wave number range 500–4500 $cm^{-1}$ and resolution 4 $cm^{-1}$. The liquid sample (oil, A0 and A200) with 0.2 mL was placed on the ATR sample holder before the data recording. The FTIR spectra were taken in a transmittance mode.

### Raman spectroscopy

Raman spectra of samples were examined using a LabRam HR800 Raman spectroscope (Horiba Jobin–Yvon, France). The Raman system was operated at 10 mV laser power and an excitation wavelength of 514 nm with an $Ar^+$ ion laser.

### Gel permeation chromatography (GPC)

Molecular weights ($M_w$ and $M_n$) and molecular weight distribution ($M_w/M_n$) of the resin were determined using a waters gel permeation chromatograph equipped with styragel column (HR series 3, 4E) and a 2410 differential refractometer detector. The analysis was performed at room temperature with purified high performance liquid chromatography grade tetrahydrofuran (THF) as eluent at 0.7 mL/min. Low polydispersed linear polystyrene standards were used to construct the calibration curve based on universal GPC calibration. Data acquisition and processing were performed using Waters Empower software package.

### X–ray absorption near edge structure (XANES)

The Cu k–edge XANES measurements were conducted at Singapore Synchrotron Light Source (SSLS), Singapore. The electron storage ring was operated with an energy of 1.3 GeV (current=100–200 mA). A Si (111) double–crystal monochromator was used for the selection of energy with an energy resolution ($\Delta E/E$) of about 1.9 x $10^{-4}$ (eV/eV). The incident photon energy was calibrated using a standard copper foil. The sample was placed inside sample holder and the spectra were recorded from 8940 to 9160 eV at ambient temperature. The linear composition fitting was conducted using Athena, a program in the IFEFITT package. The states of CuO nanoparticle before and after the reaction were determined.

### Antimicrobial test

The antimicrobial activity of the as–prepared alkyd resin samples prepared by A0 and A200 catalysts was determined by Kirby–Bauer Method[56]. A number of microorganisms, such as *Escherichia coli* (ATCC 8739)*, Pseudomonas aeruginosa* (ATCC 9027)*, Staphylococcus aureus* (ATCC6538) and *Salmonella sp.* (ATCC 14028) was considered for the experiment. The cultures were maintained in a nutrient broth and subcultured at regular intervals. The samples were prepared (10 mg/mL) using 0.5% DMSO. The microbial cultures in Nutrient agar plates were inoculated using spread plate technique and cork borer was used to make the hole on the agar. The samples (10 mg/mL) were loaded in the hole and incubated at 32.5 °C for 24 h. A blank sample was maintained separately as control. The diameter of the zone of inhibition after 24 h incubation was measured.

## Acknowledgements

## Notes and references

1.  M. R. Meneghetti and S. M. P. Meneghetti, *Catal. Sci. Technol.*, 2015, 5, 765-771.
2.  C. Aulin and G. r. Ström, *Ind. Eng. Chem. Res.*, 2013, 52, 2582-2589.
3.  S. K. Dolui, *ACS Sustainable Chem. Eng.*, 2015, 3, 261-268.

RSC Advances Accepted Manuscript

4. H. Kalita, S. Selvakumar, A. Jayasooriyamu, S. Fernando, S. Samanta, J. Bahr, S. Alam, M. Sibi, J. Vold and C. Ulven, *Green Chem.*, 2014, 16, 1974-1986.

5. C. A. Ferretti, R. N. Olcese, C. R. Apesteguía and J. I. Di Cosimo, *Ind. Eng. Chem. Res.*, 2009, 48, 10387-10394.

6. C. A. Ferretti, A. Soldano, C. R. Apesteguía and J. I. Di Cosimo, *Chem. Eng. J.*, 2010, 161, 346-354.

7. D. Doulia, S. Rokotas and K. Georgopoulou, *Surf. Coat. Int. Pt. B-C*, 2006, 89, 215-219.

8. S. Ebrahimiasl, A. Zakaria, A. Kassim and S. N. Basri, *Int. J. Nanomedicine*, 2015, 10, 217.

9. A. Kubacka, M. S. Diez, D. Rojo, R. Bargiela, S. Ciordia, I. Zapico, J. P. Albar, C. Barbas, V. A. M. dos Santos and M. Fernández-García, *Sci. Report.*, 2014, 4, 4134.

10. K. Delgado, R. Quijada, R. Palma and H. Palza, *Lett. Appl. Microbiol.*, 2011, 53, 50-54.

11. R. Brayner, R. Ferrari-Iliou, N. Brivois, S. Djediat, M. F. Benedetti and F. Fiévet, *Nano Lett.*, 2006, 6, 866-870.

12. T. Gordon, B. Perlstein, O. Houbara, I. Felner, E. Banin and S. Margel, *Colloids Surf. A: Physicochem. Eng. Asp.*, 2011, 374, 1-8.

13. M. N. K. Chowdhury, M. D. H. Beg, M. R. Khan and M. F. Mina, *Mater. Lett.*, 2013, 98, 26-29.

14. H. R. Ong, M. R. Khan, R. Ramli and R. M. Yunus, *Appl. Mech. Mater.*, 2014, 481, 21-26.

15. E. Ozkan, F. T. Ozkan, E. Allan and I. P. Parkin, *RSC Adv.*, 2015, 5, 8806-8813.

16. F. L. Pua, S. Zakaria, C. H. Chia, S. P. Fan, T. Rosenau, A. Potthast and F. Liebner, *Sains Malaysia.*, 2013, 42, 793-799.

17. H. R. Ong, R. Prasad, M. M. R. Khan and M. N. K. Chowdhury, *Appl. Mech. Mater.*, 2012, 121-126, 493-498.

18. I. O. Igwe and O. Ogbobe, *J. Appl. Polym. Sci.*, 2000, 78, 1826-1832.

19. C. A. Ferretti, S. Fuente, R. Ferullo, N. Castellani, C. R. Apesteguía and J. I. Di Cosimo, *Appl. Catal. A Gen.*, 2012, 413, 322-331.

20. A. I. Aigbodion and F. E. Okieimen, *Ind. Crops Prod.*, 2001, 13, 29-34.

21. T. E. Odetoye, D. S. Ogunniyi and G. A. Olatunji, *Ind. Crops Prod.*, 2010, 32, 225-230.

22. T. E. Odetoye, D. S. Ogunniyi and G. A. Olatunji, *Prog. Org. Coat.*, 2012, 73, 374-381.

23. I. E. Ezeh, S. A. Umoren, E. E. Essien and A. P. Udoh, *Ind. Crops Prod.*, 2012, 36, 94-99.

24. H. A. Goldsmith, *Ind. Eng. Chem.*, 1948, 40, 1205-1211.

25. A. I. Aigbodion and F. E. Okieimen, *Eur. Polym. J.*, 1996, 32, 1105-1108.

26. H. S. Fogler, *Elements of chemical reaction engineering*, Prentice Hall Professional Technical Reference USA, 4th edn., 2005.

27. V. C. Patel, J. Varughese, P. A. Krishnamoorthy, R. C. Jain, A. K. Singh and M. Ramamoorty, *J. Appl. Polym. Sci.*, 2008, 107, 1724-1729.

28. S. M. Cakić, I. S. Ristić, V. M. Jašo, R. Ž. Radičević, O. Z. Ilić and J. K. B. Simendić, *Prog. Org. Coat.*, 2012, 73, 415-424.

29. E. F. Assanvo, P. Gogoi, S. K. Dolui and S. D. Baruah, *Ind. Crops Prod.*, 2015, 65, 293-302.

30. J. Wu, T. Zhang, G. Ma, P. Li, L. Ling and B. Wang, *J. Appl. Polym. Sci.*, 2013, 130, 4201-4208.

31. Y. Xu, D. Chen, X. Jiao and K. Xue, *J. Phys. Chem. C*, 2007, 111, 16284-16289.

32. G. Gouadec and P. Colomban, *Progress in Crystal Growth and Characterization of Materials*, 2007, 53, 1-56.

33. J. Zięba-Palus, A. Michalska and A. Wesełucha-Birczyńska, *J. Mol. Struct.*, 2011, 993, 134-141.

34. J. L. Koenig and P. T. K. Shih, *Journal of Polymer Science Part A-2: Polymer Physics*, 1972, 10, 721-740.

35. M. A. Omri, A. Triki, M. Guicha, M. B. Hassen, M. Arous, H. A. El Hamzaoui and A. Bulou, *Appl. Phys. A*, 2015, 118, 1067-1078.

36. C. Liu, Z. Wang, Y. a. Huang, H. Xie, Z. Liu, Y. Chen, W. Lei, L. Hu, Y. Zhou and R. Cheng, *RSC Adv.*, 2013, 3, 22380-22388.

37. B. Marton, L. G. J. van der Ven, C. Otto, N. Uzunbajakava, M. A. Hempenius and G. J. Vancso, *Polymer*, 2005, 46, 11330-11339.

38. M. Skrifvars, P. Niemelä, R. Koskinen and O. Hormi, *J. Appl. Polym. Sci.*, 2004, 93, 1285-1292.

39. J. A. F. Pierna, V. Baeten, O. Abbas and P. Dardenne, *Biotechnology, Agronomy, Society and Environment*, 2011, 15, 75-84.

40. K. Krishnamoorthy, M. Premanathan, M. Veerapandian and S. J. Kim, *Nanotechnology*, 2014, 25, 315101.

41. K. Krishnamoorthy, K. Jeyasubramanian, M. Premanathan, G. Subbiah, H. S. Shin and S. J. Kim, *Carbon*, 2014, 72, 328-337.

42. A. I. Aigbodion and C. K. S. Pillai, *J. Appl. Polym. Sci.*, 2001, 79, 2431-2438.

43. F. E. Okieimen and A. I. Aigbodion, *Ind. Crops Prod.*, 1997, 6, 155-161.

44. M. Alam, D. Akram, E. Sharmin, F. Zafar and S. Ahmad, *Arabian Journal of Chemistry*, 2014, 7, 469-479.

45. S. K. Dhoke, T. J. M. Sinha, P. Dutta and A. S. Khanna, *Prog. Org. Coat.*, 2008, 62, 183-192.

46. J. R. Morones, J. L. Elechiguerra, A. Camacho, K. Holt, J. B. Kouri, J. T. Ramírez and M. J. Yacaman, *Nanotechnology*, 2005, 16, 2346.

47. G. Applerot, J. Lellouche, A. Lipovsky, Y. Nitzan, R. Lubart, A. Gedanken and E. Banin, *Small*, 2012, 8, 3326-3337.

48. A. Y. Booshehri, R. Wang and R. Xu, *Chem. Eng. J.*, 2015, 262, 999-1008.

49. L. T. Benov and I. Fridovich, *J. Biol. Chem.*, 1994, 269, 25310-25314.

50. J.-W. Rhim, S.-I. Hong, H.-M. Park and P. K. Ng, *J. Agric. Food Chem.*, 2006, 54, 5814-5822.

51. J. Singh and P. K. Dutta, *Journal of Macromolecular Science, Part A*, 2011, 48, 246-253.

52. H. R. Ong, M. M. R. Khan, R. Ramli, Y. Du, S. Xi and R. M. Yunus, *RSC Adv.*, 2015, 5, 24544-24549.

53. H. R. Ong, M. R. Khan, M. N. K. Chowdhury, A. Yousuf and C. K. Cheng, *Fuel*, 2014, 120, 195-201.

54. E. G. Bobalek and M. T. Chiang, *J. Appl. Polym. Sci.*, 1964, 8, 1147-1168.

55. E. G. Bobalek, E. R. Moore, S. S. Levy and C. C. Lee, *J. Appl. Polym. Sci.*, 1964, 8, 625-657.

56. S. Ambika, S. Arunachalam, R. Arun and K. Premkumar, *RSC Adv.*, 2013, 3, 16456-16468.